Vacuum 245 (2026) 114997

Contents lists available at ScienceDirect

Vacuum

journal homepage: www.elsevier.com/locate/vacuum

Effect of Ti layer on deformation ability and damage mechanism of diamond-like carbon coated aluminum alloy

Yanjin Li [a,b,1], Xin Zhang [a,1], Silong Zhang [a], Hao Li [a], Rende Chen [a], Kazuhito Nishimura [a], Peng Guo [a,*], Aiying Wang [a,b,**]

[a] State Key Laboratory of Advanced Marine Materials, Zhejiang Key Laboratory of Extreme-environmental Material Surfaces and Interfaces, Ningbo Institute of Materials Technology and Engineering, Chinese Academy of Sciences, Ningbo, 315201, China
[b] Center of Materials Science and Optoelectronics Engineering, University of Chinese Academy of Sciences, Beijing, 100049, China

ARTICLE INFO

Keywords:
Aluminum alloy
DLC coating
Ti layer
Interface structure
Damage mechanism

ABSTRACT

Ti interlayer effectively improves the protective performance of Diamond-like carbon (DLC) coatings for Al-based alloys, by compensating for their large interfacial mismatch. However, optimization of the Ti interlayer has largely remained trial-and-error approaches, because the interface behavior under external loading has not been systematically revealed. Here, DLC around 1 μm were deposited on Al alloys with Ti interlayer, whose microstructure was varied by changing its thickness from 0.15 to 0.97 μm. Results demonstrated that the thickness of Ti layer had little effect on the intrinsic structure of DLC, with a critical thickness of 0.75 μm, the Ti can effectively reduce the stress and enhance hardness of systems. Interfacial structure analysis after indentation testing affirmed that, the plastic deformation ability of Al/Ti/DLC was increased and the cracking of DLC layer towards inside was significantly suppressed. However, thin Ti layers failed to alleviate stress concentration at the Ti/DLC interface, and Ti layers thicker than the critical value developed the stronger (0002) phase orientation, which in turn sacrificed the grain boundary bonding and was destructive to its load-bearing capacity. These findings demonstrated that the Ti layer with dense structure was extremely crucial for achieving high-performance DLC coatings on Al alloys.

1. Introduction

Owning to the combined advantages of high specific strength, excellent formability, and low price, Al alloys have been increasingly used to manufacture automobile components to improve their energy efficiency [1,2]. Nevertheless, Al alloy components are susceptible to accelerated wear and failure in practical applications, owing to their inherently low hardness and inferior wear resistance. As effective solution to these challenges, various surface modification techniques have been attempted and demonstrated to enhance the comprehensive performance of aluminum alloys. For example, Chen and co-workers [3] confirmed that Al_2O_3 ceramic film prepared by micro-arc oxidation technique can reduce wear rate of 7A04 aluminum alloy by an order of magnitude. Li et al. [4] prepared TC4 titanium alloy coating on 7075 Al alloy with laser cladding method, and the coating exhibited both improved corrosion and wear resistance. A substantial body of research [5,6] found that with the high-energy ion implantation method, the surface-modified aluminum alloys exhibited lower and reduced weight loss in the wear tests, besides, nitrogen ion implantation can also provide long-term corrosion protection for aluminum alloys.

In particular, diamond-like carbon (DLC) coating is one of the most promising candidates owning to its high hardness, solid-lubricant properties and excellent corrosion resistance [7,8], which can significantly broaden the operational limits of aluminum alloy components, particularly in severe wear and corrosive conditions. However, the poor chemical affinity between C and Al leads to weak adhesion strength between DLC and Al alloys. Besides, the high internal residual stress in DLC up to several GPa, and its much higher hardness/modulus compared to Al alloys can cause premature fracture and adhesion failure due to the “eggshell effect” [9]. So, choosing the appropriate transition

* Corresponding author.
** Corresponding author. State Key Laboratory of Advanced Marine Materials, Zhejiang Key Laboratory of Extreme-environmental Material Surfaces and Interfaces, Ningbo Institute of Materials Technology and Engineering, Chinese Academy of Sciences, Ningbo, 315201, China.
E-mail addresses: guopeng@nimte.ac.cn (P. Guo), aywang@nimte.ac.cn (A. Wang).
[1] These authors contributed equally to this work.

https://doi.org/10.1016/j.vacuum.2025.114997
Received 21 September 2025; Received in revised form 25 November 2025; Accepted 6 December 2025
Available online 8 December 2025

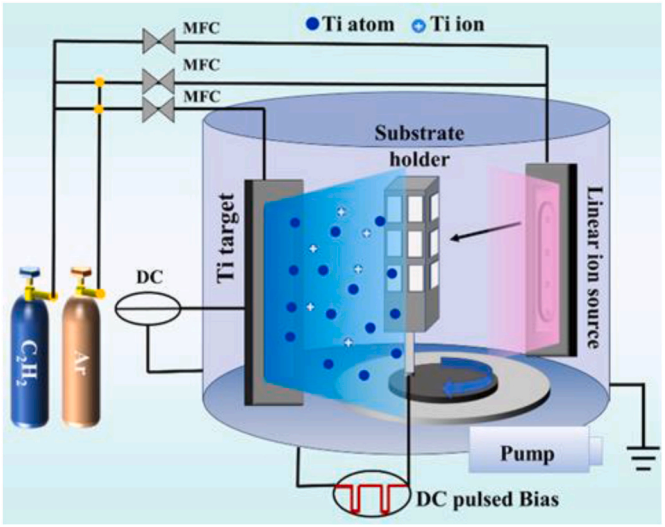

Fig. 1. The schematic diagram of the DCMS equipment.

layer to mitigate the chemical and mechanical misfit between DLC and Al alloys is the prerequisite for practical application of DLC coated Al alloy.

Considering the combined requirements, Ti buffer layer is anticipated to enhance the adhesion strength and protective performance of the DLC coatings on Al alloys. Firstly, Ti layer has good chemical affinity with both Al and C [10–12], in addition, the Ti layer can simultaneously form strong metallic bonds with the Al substrate and generate a thin TiC transition phase with carbon, thereby promoting robust interfacial adhesion. As well as a medium coefficient of thermal expansion (8.6×10^{-6}/K) between that of DLC (2.3×10^{-6}/K) and Al alloys (23.2×10^{-6}/K), therefore, the Ti layer can mitigate interfacial thermal stresses. Moreover, Ti layer could decrease the distortion of the bond angle and bond length [13], catalyze the conversion from sp^3 bonding to sp^2 bonding, thereby alleviating residual stress in DLC. For example, Wang et al. [14]and Maruno et al. [15] found that the internal stress of DLC exhibited about 30 % reduction by introducing Ti layer. Cao et al. [16] also reported that with Ti layer, the residual stress of Ti-DLC on Al alloys decreased from 12.4 GPa to 2.4 GPa, meanwhile, the adhesion strength increased from 12.8 N to 42 N.

What's more critical, the Ti layer can significantly improve the deformation ability and load-bearing capacity of the DLC coated Al alloys, combined with its moderate hardness and elastic modulus. For example, Liao et al. [17] showed that the insertion of Ti layer can disperse the contact stress and prevent crack expansion in DLC coated 2024 Al alloys, with large applied load of 20 N. Similarly, Cao and co-workers [18] prepared a multilayer DLC composed of alternating Ti and Ti-DLC layers on Al alloy, and the optimized coating displayed a large thickness of ~17 μm, low friction coefficient (~0.13), low wear rate (1.0×10^{-7} mm^3/Nm) and high adhesion strength of 15.6 N.

Essentially, the deformation behaviors and crack resistance of Ti layer greatly decides protective performance of the hard DLC on relatively soft substrates. As reported by Jang et al. [19] in the tensile testing, compared with columnar Ti layer, the dense Ti layer reduced the wear rate and inhibited crack generation of DLC coated ductile substrates. Unfortunately, without detailed in-situ interfacial analysis, the role of thickness, grain size, and crystallographic orientation of the Ti layer on load-bearing capacity and damage mechanism of DLC coated Al alloy remains unresolved.

In this paper, to investigate the effect of Ti layer, DLC coatings with different Ti layer thickness were deposited on Al alloy by DC magnetron sputtering, in regard to thickness-induced microstructural modification in the Ti layer, including its important role on interfacial stress, structural continuity, and damage tolerance [20]. The interfacial evolution of the DLC coated Al alloy under indentation was systematically investigated, the plastic deformation ability and the related damage mechanism were discussed. Specifically, the thickness-dependent microstructural evolution of Ti interlayers and its direct correlation with the interfacial deformation and damage mechanisms was clarified, which can provide critical understanding and theoretical guidance for transition layer design of DLC-based coatings for Al alloy protection.

2. Experimental details

2.1. Coating deposition

The Ti/DLC coating was deposited on Al (6061-T6) substrates in a size of 20 mm × 15 mm × 3 mm and Si wafers with thickness of 500 μm, by using linear ion source composited DC magnetron sputtering equipment (Fig. 1). Before deposition, the substrates were polished to mirror finish, and cleaned in an ultrasonic bath using acetone and ethanol for 10 min in order to remove the surface contaminants. The base vacuum of the deposition chamber was better than 3×10^{-5} Torr. Substrates were etched by Ar ion for 40 min prior to the deposition process to further remove surface oxides and contaminants, with Ar flow rate of 38 sccm, the pulsed bias voltage of −200 V and the working pressure of 0.3 Pa. Then, the Ar gas (48 sccm) was introduced to the chamber to inspire the titanium target (99.99 %) with the DC sputtering power of 1.1 kW, a substrate bias of 200 V, and the working pressure of 0.4 Pa for Ti layer deposition. All coatings were deposited at room temperature. Based on thickness measurements using a stylus profilometer, the deposition rate of the Ti layer was approximately 15 nm/min, and its thickness was controlled by adjusting the deposition time to 10, 20, 30, 40, 50, and 60 min, respectively. The DLC coating with an average thickness of 1 μm was prepared by linear ion source of 0.24 kW, with a C_2H_2 flow rate of 35–38 sccm, a substrate bias of −100 V and a working pressure of 0.3 Pa. During the deposition process, the sample was rotated at 10 rpm to ensure high uniformity of the coating.

2.2. Characterization

The surface and cross-sectional morphology of the as-deposited coating was analyzed by field emission scanning electron microscopy (SEM, Hitachi S-4800). Raman spectroscopy (inVia-reflex, Renishaw) was employed to evaluate the carbon atomic bonding states of the coatings. The wavelength of the laser was 532 nm and the wavenumber range for analysis was from 800 to 2000 cm^{-1}. The phase composition and crystal structure of the as-deposited and annealed coatings were characterized using X-ray diffraction (XRD; D8 Advance, Bruker) with Cu Kα radiation. The scans were performed over a 2θ range of 5–90° with a step size of 0.02°.

The residual stress of the coatings was evaluated using the Stoney equation:

$$\sigma = Es \cdot ts^2 \,/\, [6 \cdot (1 - \nu s) \cdot tf \cdot R]$$

where σ is the residual stress of the film, Es and νs are the Young's modulus and Poisson's ratio of the substrate, respectively, ts and tf represent the substrate and film thicknesses, and R is the radius of curvature of the substrate. The curvature R was measured using a laser reflection method.

Nano-indentation test was performed on G200 equipment with a Berkovich indenter using continuous stiffness mode. The Oliver and Pharr method was employed to calculate hardness (H) and elastic modulus (E) [21]. The residual stress of coatings was calculated by the Stoney formula [22]. The curvature of samples was measured by the stress tester using a laser reflection method. Vickers indentation test was performed on the coatings with 50g external concentrated load, with subsequent crack propagation analysis via SEM and transmission electron microscopy (TEM, Talos F200x). The sample after indentation test

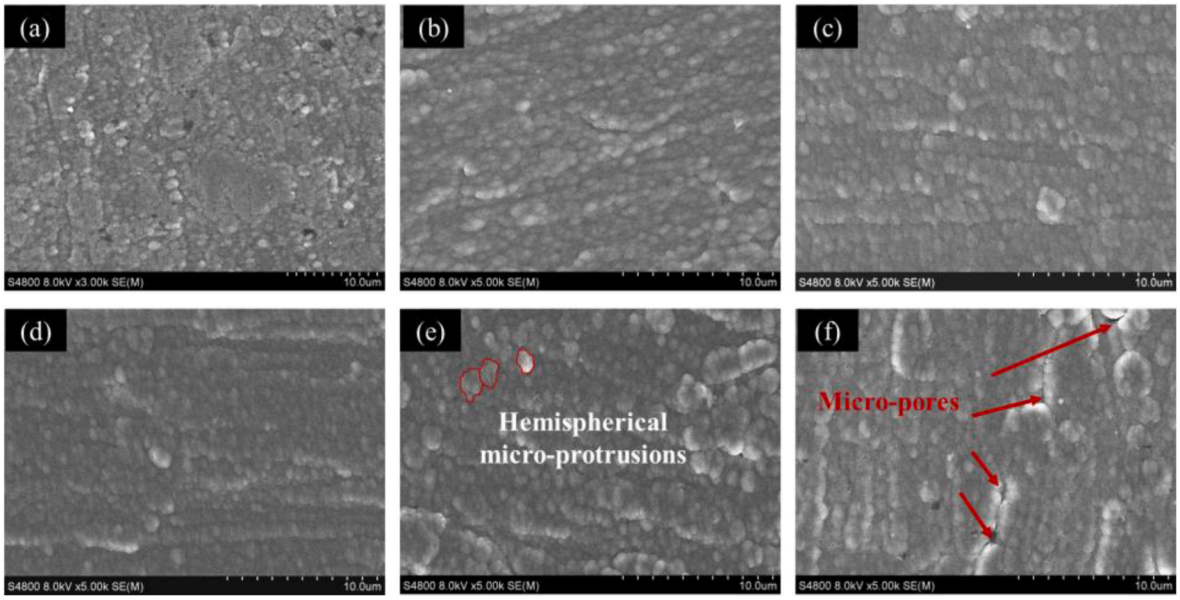

Fig. 2. Surface morphology of DLC with different Ti interlayer deposition time of (a) 10 min, (b) 20 min, (c) 30 min, (d) 40 min, (e) 50 min, (f) 60 min, respectively.

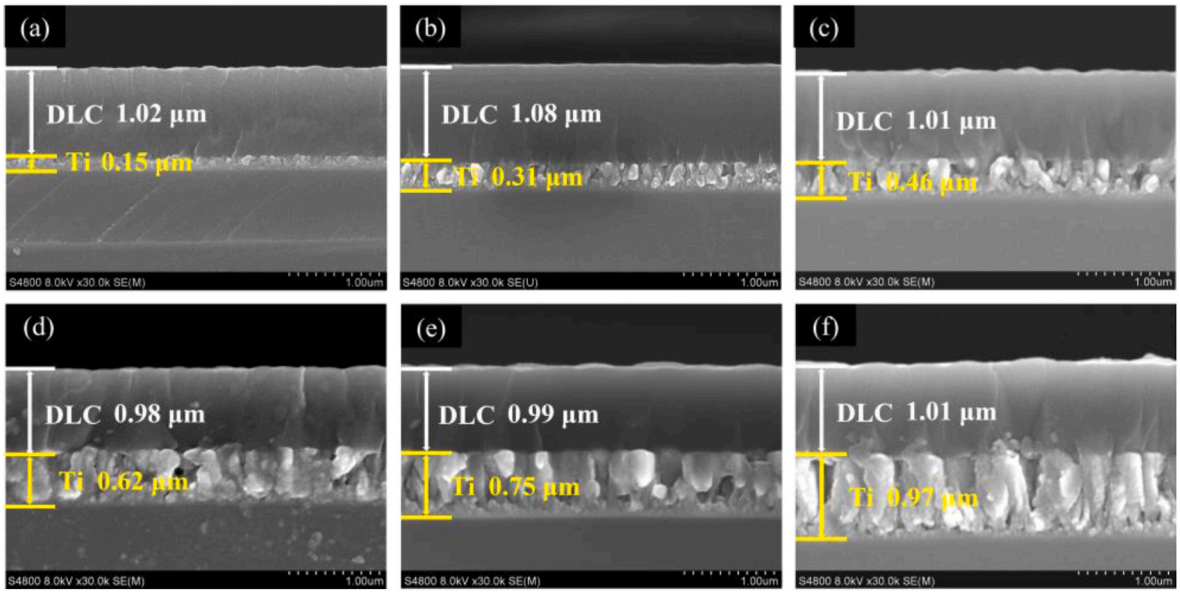

Fig. 3. Cross-sectional morphology of DLC with different Ti interlayer thickness.

for cross-sectional morophology TEM observation was prepared by using a focused ion beam (FIB, Carl Zeiss, Auriga).

3. Result and discussion

3.1. Surface and cross-sectional morphology

As shown in Fig. 2, compared with single Ti layer (Supplementary Material), the as-deposited coatings present the similar dense surface morphology with Ti interlayer deposition time range from 10 min to 50 min, exhibiting closely packed micro-protrusions (as indicated by red circles in Fig. 2e), while, when Ti interlayer deposition time reaches 60 min, some micro-pores (as marked by red arrows in Fig. 2f) are distributed along the few cracks. Usually, the grain size-thickness correlation for thin films may cause wide inter-columnar gaps and raise the roughness of bottom Ti layer [23,24], the following DLC coating will inherit the surface morphology characteristics and its growth process may also significantly be influenced by the possible grain coarsening of the Ti layer [25].

Fig. 3 shows a cross-sectional view of the DLC coatings on Si wafers. The thickness of the Ti interlayer is 0.15 μm, 0.31 μm, 0.46 μm, 0.62 μm, 0.75 μm, and 0.97 μm, respectively. While the thickness of DLC is maintained at about 1 μm. Clearly, all Ti interlayers show typical columnar structure, with increasing thickness, the grain size in the Ti layer becomes larger and more micro-voids appear. Besides, the Si-Ti and Ti-DLC interfaces are intact and dense, indicating well adhesion between the coating and the substrate, as shown in the scratch tests (Supplementary Material).

3.2. XRD and Raman spectroscopy

XRD patterns in Fig. 4 confirm that only the α-Ti (HCP) structure can

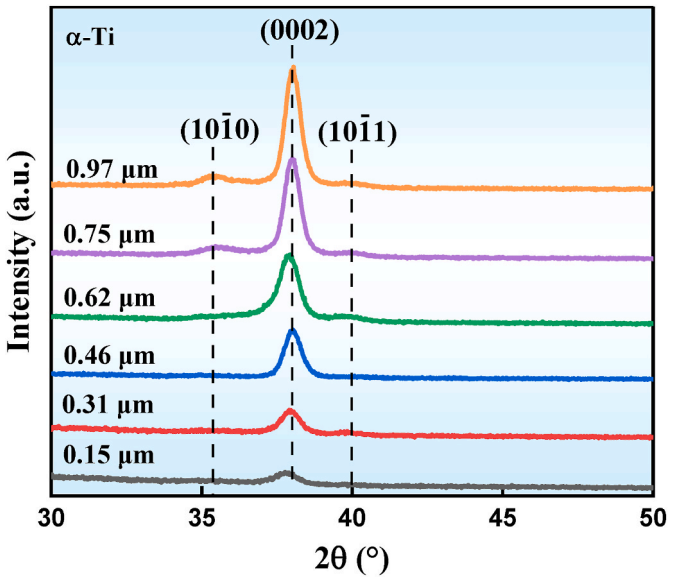

Fig. 4. XRD pattern of DLC samples with Ti interlayer thickness from 0.15 to 0.97 μm, respectively.

be detected and all samples show strong (0002) preferred orientation. The intensities of all diffraction peaks, including weak (10 $\bar{1}$ 0) and (10$\bar{1}$ 1) peaks, become evidently as the Ti interlayer thickness increases. The preferred (0002) orientation in the Ti layer may result from the competition of surface and strain energy during the PVD process. For DC magnetron sputtering, the low-ionization plasma yields low adatom energy, that leads to a small strain energy of the Ti layer. Therefore, the reduction of surface energy could be the main driving force to forge crystallographic orientation of the columnar grain. With thickness rising, the Ti layer grows along the plane with the lowest surface energy [26], namely, the (0002) plane for α-Ti [27], resulting in strong (0002) preferred orientation in the XRD patterns.

The typical G and D peak bonding characteristics of DLC fitted in Gaussians mode are probed by Raman spectroscopy, as shown in Fig. 5a. For all samples, the asymmetric peak appears in the range of 800~2000 cm^{-1}, and the typical D and G peaks lie at near 1350 cm^{-1} and 1560 cm^{-1} [28], respectively. The full width at half maximum of the G band peak (G_{FWHM}), the G peak position, and the relative intensity ratio of the D and G bands (I_D/I_G) obtained from the ratio of peak area are used to describe the structure of DLC. The shift in I_D/I_G and G peak position indicates a change in the average size and quantity of sp^2 clusters, the G_{FWHM} is a measurement of the bond length and bond angle disorder. In Fig. 5b, as the thickness of the Ti interlayer increases from 0.15 to 0.97 μm, G_{FWHM}, I_D/I_G, and the position of G peak of all samples practically remain stable at almost around 180 cm^{-1}, 1.1, and 1542 cm^{-1}, respectively, indicating a similar sp^2 hybridization percentage, structural disorder, and the sp^2 cluster size in the upper DLC.

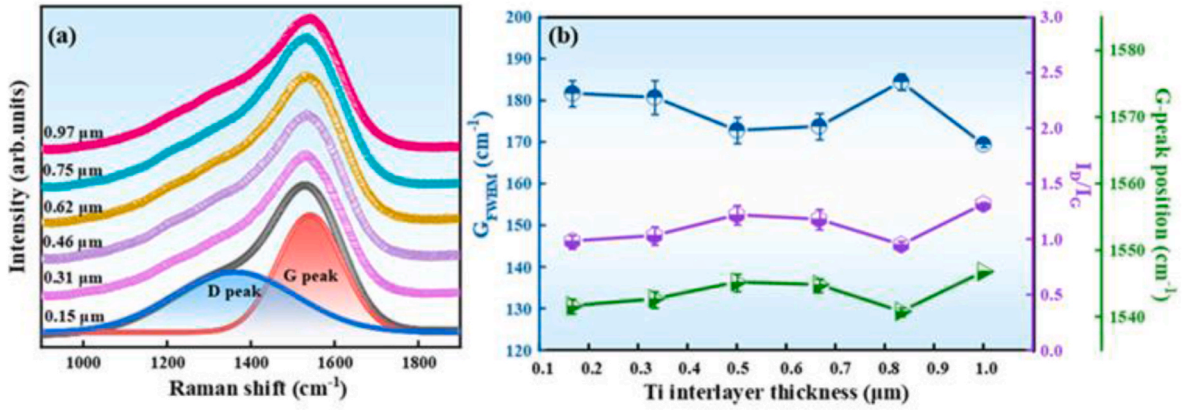

Fig. 5. (a) Raman spectra of all samples; (b) G_{FWHM}, I_D/I_G, position of G peak in the upper DLC.

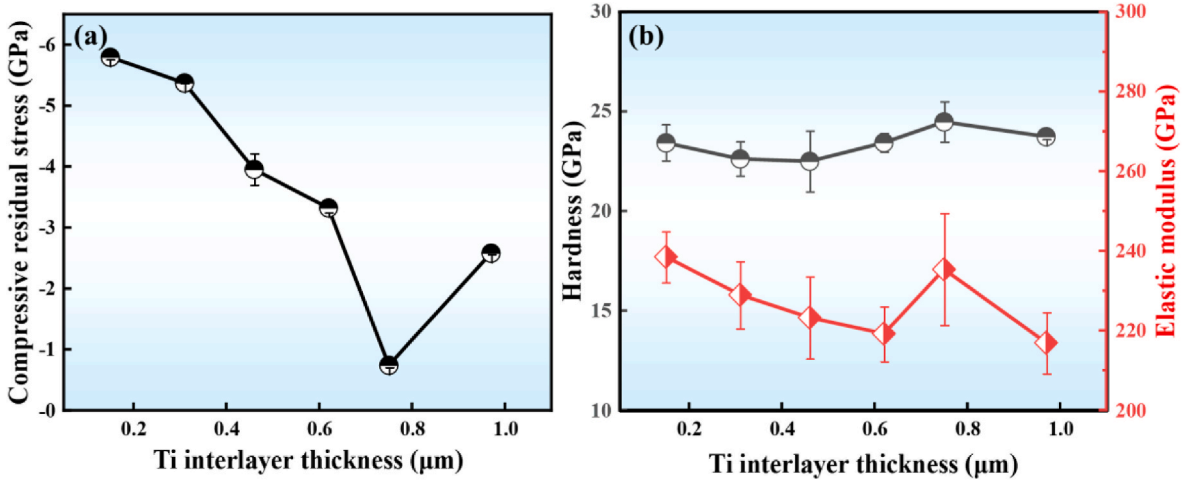

Fig. 6. (a)Residual stress; (b)Hardness and modulus of samples with different Ti interlayer thickness.

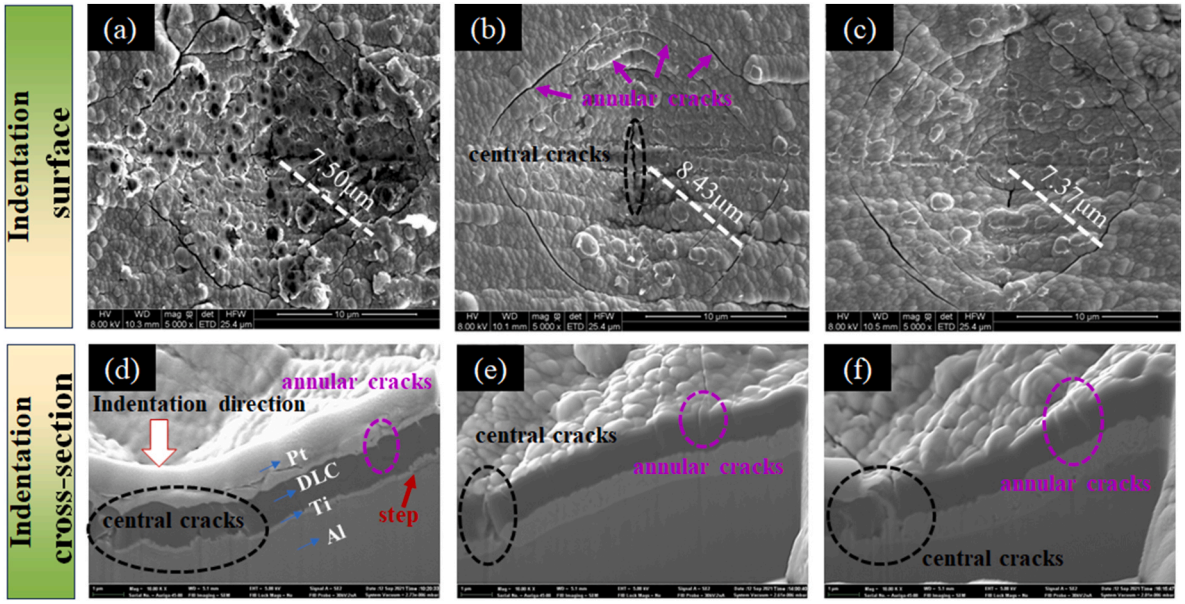

Fig. 7. The surface and cross-sectional morphology of indentation of sample with Ti layer thickness of (a), (d) 0.15 μm, (b), (e) 0.75 μm, (c), (f) 0.97 μm, respectively.

3.3. Mechanical properties

Due to the mixed sp^2 and sp^3 C-C and sp^3 C-H bonding structures, DLC has a high-level intrinsic internal compressive stress, which is one of the primary reasons for its brittleness. Fig. 6a shows the residual stress of the coatings. As the thickness of Ti layer increases from 0.15 μm to 0.75 μm, the residual stress first decreases dramatically from its maximum value of 5.82 GPa–0.71 GPa, then increases to 2.58 GPa when thickness further increases to 0.97 μm. Therefore, Ti interlayer with a critical thickness of 0.75 μm can effectively reduce the compressive residual stress of DLC.

Both growth stress and thermal stress are components of residual stress. While, the Ti/DLC coatings were deposited at room temperature to avoid significant thermal effect, yielding a very weak impact of thermal stress, which was further buffered by Ti interlayer [29], therefore, the effect of thermal stress can be ignored reasonably in this case. Generally, due to low adatom energy in DC magnetron plasma and diffusivity coefficient of Ti, mobility of Ti atoms is sufficiently low, yielding a tensile stress state of Ti layer as a result of grain boundary (GB) attraction [30]. Meanwhile, columnar grains rapidly coarsen along the preferred (0002) planes in horizontal direction, forming strong shadowing effect blocking incoming adatoms, creating micro-voids and cracks, as shown in Fig. 2, which in turn releases the tensile stress provided by Ti layer. When thickness exceeds the critical value (0.75 μm), tensile stress starts to decrease, leading to the back-bounding of compressive stress. Because its microstructure evolves into coarsened columnar grains with partial porosity, which relaxes the intrinsic tensile growth stress; meanwhile, the less-densified upper region becomes more sensitive to ion peening during DLC deposition, causing compressive stress accumulation [31]. As a result, the overall residual tensile stress decreases and a compressive-stress rebound appears.

Fig. 6b shows the nano-hardness and elastic modulus of all samples. Compared with DLC, the hardness of Ti interlayer is low, as shown in Supplementary Material. With the thickness of the Ti layer, the hardness first decreases from 23.4 ± 0.9 GPa to 22.5 ± 1.5 GPa, then increases to 24.5 ± 1.0 GPa. The elastic modulus shows the same tendency. In this thickness range of Ti layer, the sample with Ti layer thickness of 0.97 μm shows lower hardness and elastic modulus (23.7 ± 0.1 GPa and 216.9 ± 7.6 GPa). The sample with 0.75 μm Ti layer has the highest hardness and elastic modulus.

The hardness and elastic modulus are impacted by both the stress state of the entire coating and the thickness of Ti layers. Firstly, the decreasing trend of hardness and elastic moduli as the thickness of Ti interlayer increases from 0.15 μm can be rationalized by the decreasing compressive stress [32]. When the Ti interlayer thickness further increases to 0.75 μm, thickness of the interlayer may overwhelm the compressive stress factor. A relatively dense and thick Ti interlayer provides strong support for DLC layer, causing dramatic increase of hardness and elastic modulus. When the thickness surpasses 0.75 μm, Ti interlayer becomes loose, as shown in Fig. 2, so that supporting effect drops sharply, leading to an obvious decrement of hardness and elastic modulus at 0.97 μm [33].

3.4. Indentation behavior and damage mechanism of coatings

In consideration of the “eggshell effect”, the deformation behaviors of Ti layer is one of the main factors to determinate the load carrying ability of the hard DLC coating. To reveal the related damage mechanism, three typical samples with small (0.15 μm), medium (0.75 μm) and large (0.97 μm) Ti interlayer thickness are selected for Vickers indentation testing.

Overall, the DLC layers exhibit unambiguously brittle behaviors due to the covalent nature of C-C and C-H bonding, in addition, the DLC toplayer has much higher elastic modulus, so effect alike stress shielding [34] is thus rendered and causes stress concentration inside DLC layers and the consequent cracking. From the surface micrographs of indentations in Fig. 7a, b, and 7c, the three samples display similar tetragonal pyramidal shape, the distances between the indentation boundaries and the central point are 7.5 μm, 8.43 μm, and 7.37 μm, as indicated by the white lines, meanwhile, two types of cracks, namely, annular cracks (indicated by the purple arrows circle) at the edge of the indentation and central cracks (indicated by the black circle) at the core area of the indentation can be observed. Besides, compared with sample with 0.75 μm Ti layer, the two samples with 0.15 μm and 0.97 μm Ti layer exhibit pronounced material pile-up at indentation peripheries.

In Fig. 7d, e, f, the corresponding cross-sectional morphology of the indented area is taken from the right part of the imprint for direct observation of the cracking behavior. Comparable indentation depths of 3.18 μm, 3.15 μm, and 3.20 μm are recorded for the three specimens respectively, suggesting the distinct edge deformation of Al alloy, Ti layer, and DLC coating. Besides, the annular cracks primarily initiate from the surface of DLC layers, due to the concentration of tensile stress

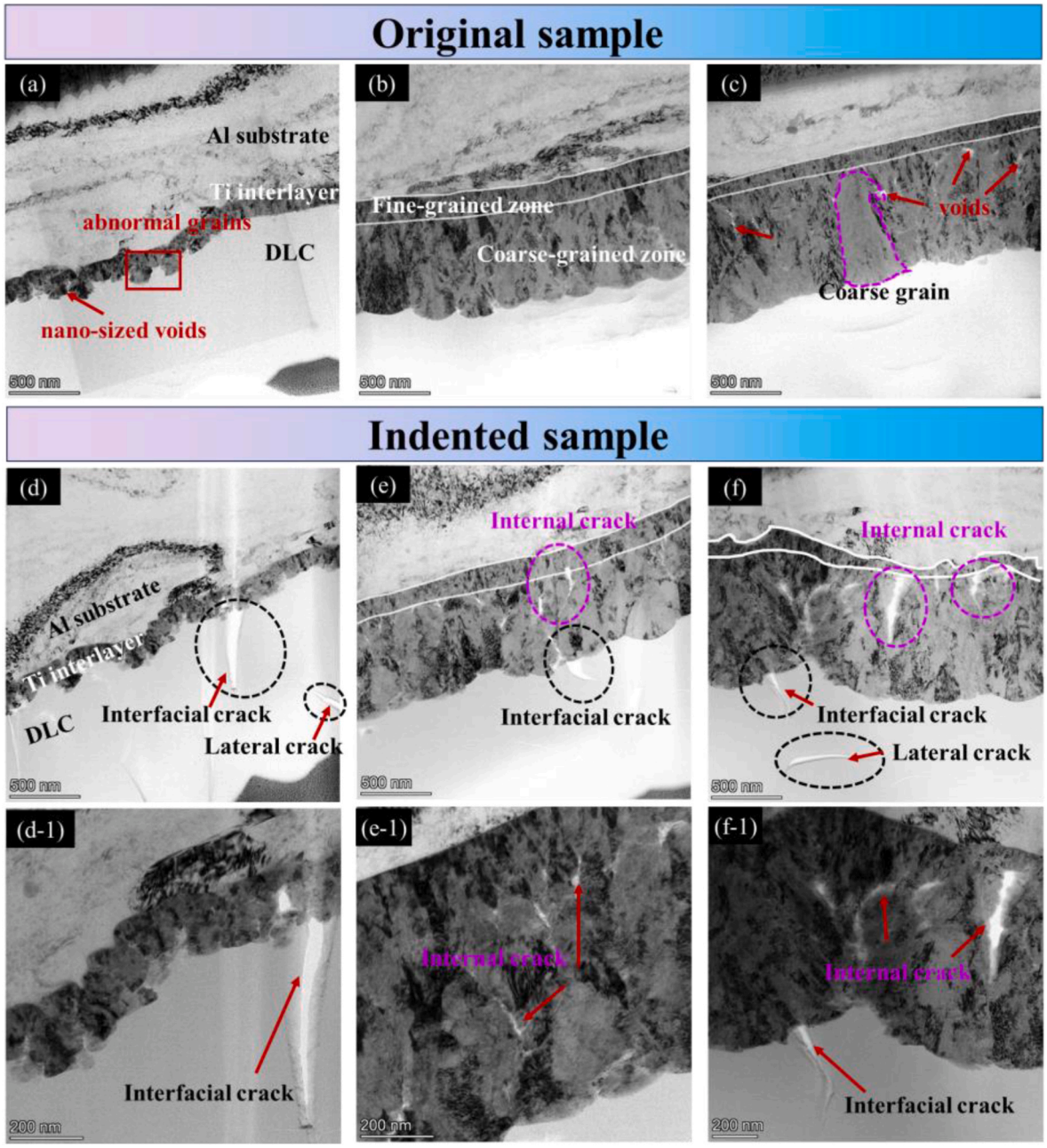

Fig. 8. (a), (b) and (c): TEM Cross-sectional morphology of as-deposited sample with Ti layer thickness of 0.15 μm, 0.75 μm, 0.97 μm, respectively; (d), (e) and (f): Cross-sectional morphology of indented samples with Ti layer thickness of 0.15 μm, 0.75 μm, 0.97 μm, respectively; (d-1), (e−1) and (f-1) correspond to the magnified images shown in Figures (d), (e), and (f).

combined with severe vertical shear facilitated by the bending of the indentation edge under the surface tension, as indicated by the purple circle. While, the central cracks propagate in an extremely wide manner, and are more concentrated in the interfacial zone, as indicated by the black circle, where the cracks first initiate at the Ti/DLC interface and grow up through the DLC layer, as a result of the maximum shear sliding of the DLC layer to deform coordinately with the indenter that press downward during the loading process.

Though, the Ti interlayer cannot prevent cracking initiation in the top of DLC layer, but to some extent, it effectively suppresses cracking propagation and promotes step formation at the Ti/DLC interface, as shown by the red arrow in Fig. 7d–f. With the minimal thickness of Ti layer in Fig. 7d, the interfacial region exhibits more curved structures and moderate extrusion of the Ti layer. For the sample with a thickness of 0.97 μm Ti layer, significant extrusion of the Ti layer appears at the Ti/DLC interface in Fig. 7f. For the sample with moderate thickness of 0.75 μm Ti layer, the highest density of cracking and steps can be observed at the interface, which may result in its best performance.

To systematically investigate the interfacial microstructure evolution induced by indentation, the coated Al alloy before and after indentation testing is investigated by TEM. For the as-deposited samples, in Fig. 8a, the 0.15 μm Ti interlayer has a dense and fine ungrown structure, with some abnormal grown grains, as marked by red frames, and few nano-sized voids appear, indicated by red arrows. Comparatively, the 0.75 μm Ti layer in Fig. 8b shows a distinct V-shaped columnar morphology resulted from speeding-up growth along (0002) planes, with few opened GBs or cracks formed in the interfacial region. As the Ti layer thickness reaches 0.97 μm (Fig. 8c), the columnar grains grow coarser, and a number of voids and cracks are formed between GBs due to shadowing effect.

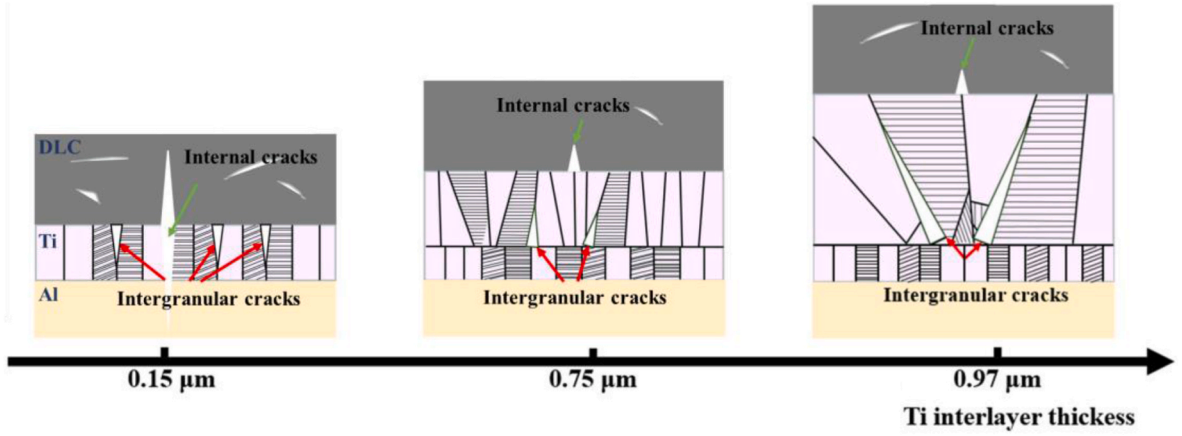

Fig. 9. Schematic of failure mechanism for DLC coated Al alloy.

After indentation testing, Fig. 8d, e, and f show the corresponding deformation structure, which clearly demonstrates that the brittle DLC layer deforms via cracking, while the ductile Ti layer and Al alloy basically deform in a typical plastic manner. To facilitate a clearer observation of the crack morphologies and propagation path, key regions are magnified in Fig. d, e, f and designated them as Fig. d-1, e−1, f-1. There are two types of cracking source, from the Ti/DLC interface (indicated by the black circle) and internal cracks in the Ti layer (indicated by the purple circle). In Fig. 8d and d-1, the sample with thinnest Ti interlayer shows most severe cracking morphology with respect to crack numbers and length, with longest crack more than 500 nm initiated from Ti/DLC interface, especially. The interfacial cracks along boundary between Ti layer and DLC, and the lateral cracks in the DLC become smaller and shorter as Ti interlayer grows thicker, as shown in Fig. 8 e, e−1 & f, f-1.

According to the mechanical properties, and interfacial evolution during indentation testing, the deformation behaviors and damage mechanism of DLC coated Al alloy should be discussed from its growth characteristic and morphology of Ti layer with increasing thickness. For deposition of Ti layer, the preferred (0002) planes in horizontal direction are promoted with increasing thickness, as shown in XRD Fig. 4, besides, more voids and cracks are formed, due to the columnar grain growth characteristics of Ti layer, as shown in Fig. 8a and b and c, which in turn releases the tensile stress provided by Ti layer in Fig. 6a.

While, within the thinnest Ti interlayer, its dense structure and few nano-sized voids may result in more curved structures at the Ti/DLC interfacial region, but this Ti layer is too thin to prevent extrusion of the Al alloy substrate with large plastic deformation, and the following large deformation of Ti layer can cause large-scale cracks (red arrows) along Ti/DLC interface. During the subsequent successive growth of Ti layer to around 0.75 μm, the Ti layer can mitigate interfacial stress concentration from extrusion of the Al alloy substrate, moreover, with increasing Ti layer thickness, the preferred (0002) planes leads to lateral growth of columnar grains and formation of V-shaped columnar crystals in the Ti layer to a lesser extent, but the Ti layer still has relatively dense structure, some cracks can be formed insides the Ti layer and at the Ti/DLC interfacial region to reduce internal stress, and the top DLC possesses a relatively intact structure, resulting in enhanced load-bearing capacity. When the Ti layer exceeds a certain thickness, the excessively large grains cause much more cracks at grain boundaries in the Ti layer, as marked by green arrows, and the indentation process will result in more and large cracks both in Ti layer and DLC layer, exhibiting deteriorated performance. The damage mechanism diagram of DLC coated Al alloy with various Ti layer thickness is illustrated in Fig. 9.

4. Conclusion

In this work, we perform comprehensive investigations and in-depth discussions on the effects of Ti transition layer thickness on the mechanical properties and deformation mechanisms of the Al alloy-Ti/DLC coating system. The results show that Ti interlayers can effectively buffer the chemical and mechanical mismatch between DLC and Al alloys, leading to concurrent relief of residual stress and increase of hardness within a critical thickness. Whereas, Ti layers deposited by DC magnetic sputtering tend to form loose columnar GBs as a result of highly preferred (0002) growth and low adatom mobility, that are destructive to the load-bearing capacity of Ti interlayers. Therefore, a Ti interlayer with optimal thickness and dense structure is necessary for acquiring improved mechanical performance for DLC coatings for Al alloy protection, which could be achieved via tuning crystallographic orientation and microstructure of Ti layers using high-ionization deposition. The current results clarify the impacts of thickness and microstructure of Ti interlayers on Al alloy/DLC coatings and provide guidance for metallic interlayer design of hard protective coatings for soft metal substrates.

CRediT authorship contribution statement

Yanjin Li: Writing – original draft, Visualization, Validation, Investigation, Formal analysis, Data curation, Conceptualization. **Xin Zhang:** Visualization, Investigation, Formal analysis, Data curation. **Silong Zhang:** Visualization, Investigation, Formal analysis, Data curation. **Hao Li:** Writing – review & editing, Formal analysis. **Rende Chen:** Investigation. **Kazuhito Nishimura:** Investigation. **Peng Guo:** Writing – review & editing, Visualization, Project administration, Investigation, Funding acquisition, Conceptualization. **Aiying Wang:** Writing – review & editing, Validation, Project administration, Funding acquisition.

Declaration of competing interest

The authors declare that they have no known competing financial interests or personal relationships that could have appeared to influence the work reported in this paper.

Acknowledgments

This work was financial supported by the Strategic Priority Research Program of the Chinese Academy of Sciences (XDB1210402), National Science Foundation of China (U24A2030, 52471105), Zhejiang Lingyan Research and Development Program (2024C01159), and Major Special Project of Ningbo (2024Z134).

Appendix A. Supplementary data

Supplementary data to this article can be found online at https://doi.org/10.1016/j.vacuum.2025.114997.

Data availability

No data was used for the research described in the article.

References

[1] T. Dursun, C. Soutis, Recent developments in advanced aircraft aluminium alloys, Mater. Des. 56 (2014) 862–871, https://doi.org/10.1016/j.matdes.2013.12.002.

[2] J. Yang, B. Liu, D. Shu, Q. Yang, T. Hu, Vehicle giga-casting Al alloys technologies, applications, and beyond, J. Alloys Compd. (2025) 1013, https://doi.org/10.1016/j.jallcom.2025.178552.

[3] X. Chen, H. Song, H. Pu, R. Zheng, M. Zhang, D. Zhang, Study of wear and corrosion resistance of ATO nanoparticle–doped micro-arc oxide film layers, Int. J. Appl. Ceram. Technol. 21 (2023) 1078–1093, https://doi.org/10.1111/ijac.14599.

[4] X. Li, K. Wang, B. Jiang, Y. Chen, Z. Zhang, K. Lu, X. Liang, Enhancing corrosion and wear resistance of a 7075 aluminum alloy via depositing TC4 coating, J. Mater. Res. Technol. 32 (2024) 1736–1748, https://doi.org/10.1016/j.jmrt.2024.08.037.

[5] N.K. Krioni, A.A. Mingazheva, A.D. Mingazhev, Increasing the wear resistance of machine parts made of aluminum alloys by ion nitriding with high-energy activation, J. Frict. Wear 45 (2024) 45–49, https://doi.org/10.3103/s1068366624700077.

[6] O. Yu Usanova, A.V. Ryazantseva, I.L. Savelev, V.S. Timohin, Effect of ion implantation on the properties of implantable aluminum alloys, J. Phys. Conf. 1515 (2020), https://doi.org/10.1088/1742-6596/1515/2/022074.

[7] Y.S. Zou, K. Zhou, Y.F. Wu, H. Yang, K. Cang, G.H. Song, Structure, mechanical and tribological properties of diamond-like carbon films on aluminum alloy by arc ion plating, Vacuum 86 (2012) 1141–1146, https://doi.org/10.1016/j.vacuum.2011.10.019.

[8] N. Srinivasan, L.K. Bhaskar, R. Kumar, S. Baragetti, Residual stress gradient and relaxation upon fatigue deformation of diamond-like carbon coated aluminum alloy in air and methanol environments, Mater. Des. 160 (2018) 303–312, https://doi.org/10.1016/j.matdes.2018.09.022.

[9] E. Bemporad, M. Sebastiani, D. De Felicis, F. Carassiti, R. Valle, F. Casadei, Production and characterization of duplex coatings (HVOF and PVD) on Ti–6Al–4V substrate, Thin Solid Films 515 (2006) 186–194, https://doi.org/10.1016/j.tsf.2005.12.058.

[10] K. Wang, H. Zhou, K. Zhang, X. Liu, X. Feng, Y. Zhang, G. Chen, Y. Zheng, Effects of Ti interlayer on adhesion property of DLC films: a first principle study, Diam. Relat. Mater. 111 (2021), https://doi.org/10.1016/j.diamond.2020.108188.

[11] J.-G. Yao, R.K. Pan, D.F. Yin, Y. Jiang, H. Li, Microstructures and characteristics of Ti/Al interface with segregated Si element, Chin. J. Phys. 62 (2019) 296–303, https://doi.org/10.1016/j.cjph.2019.10.008.

[12] Y. Qi, L.G. Hector, N. Ooi, J.B. Adams, A first principles study of adhesion and adhesive transfer at Al(111)/graphite(0001), Surf. Sci. 581 (2005) 155–168, https://doi.org/10.1016/j.susc.2005.02.048.

[13] X. Li, P. Ke, A. Wang, Probing the stress reduction mechanism of diamond-like carbon films by incorporating Ti, Cr, or W carbide-forming metals: ab initio molecular dynamics simulation, J. Phys. Chem. C 119 (2015) 6086–6093, https://doi.org/10.1021/acs.jpcc.5b00058.

[14] P. Wang, X. Wang, T. Xu, W. Liu, J. Zhang, Comparing internal stress in diamond-like carbon films with different structure, Thin Solid Films 515 (2007) 6899–6903, https://doi.org/10.1016/j.tsf.2007.02.069.

[15] H. Maruno, A. Nishimoto, Adhesion and durability of multi-interlayered diamond-like carbon films deposited on aluminum alloy, Surf. Coating. Technol. 354 (2018) 134–144, https://doi.org/10.1016/j.surfcoat.2018.08.094.

[16] H. Cao, F. Qi, X. Ouyang, N. Zhao, Y. Zhou, B. Li, W. Luo, B. Liao, J. Luo, Effect of Ti transition layer thickness on the structure, mechanical and adhesion properties of Ti-DLC coatings on aluminum alloys, Materials 11 (2018), https://doi.org/10.3390/ma11091742.

[17] J.X. Liao, L.F. Xia, M.R. Sun, W.M. Liu, T. Xu, Q.J. Xue, The tribological properties of a gradient layer prepared by plasma-based ion implantation on 2024 aluminum alloy, Surf. Coating. Technol. 183 (2004) 157–164, https://doi.org/10.1016/j.surfcoat.2003.10.003.

[18] H. Cao, F. Liu, H. Li, F. Qi, X. Ouyang, N. Zhao, B. Liao, High temperature tribological performance and thermal conductivity of thick Ti/Ti-DLC multilayer coatings with the application potential for Al alloy pistons, Diam. Relat. Mater. 117 (2021) 108466, https://doi.org/10.1016/j.diamond.2021.108466.

[19] Y.J. Jang, J.W. Jang, J.I. Kim, W.S. Kim, M.H. Kim, J. Kim, Tensile testing as alternative evaluation method for enhanced adhesion of diamond-like carbon coatings with different titanium buffer layers, J. Mater. Res. Technol. 29 (2024) 1579–1589, https://doi.org/10.1016/j.jmrt.2024.01.105.

[20] B. Zhou, Z. Liu, A.V. Rogachev, D.G. Piliptsou, B. Tang, Size effect in the titanium/diamond-like carbon bilayer films: effect of relative thickness on their structure and mechanical properties, Surf. Interface Anal. 49 (2016) 47–54, https://doi.org/10.1002/sia.6056.

[21] W.C. Oliver, G.M. Pharr, An improved technique for determining hardness and elastic modulus using load and displacement sensing indentation experiments, J. Mater. Res. 7 (2011) 1564–1583, https://doi.org/10.1557/jmr.1992.1564.

[22] P. Wang, X. Wang, Y. Chen, G. Zhang, W. Liu, J. Zhang, The effect of applied negative bias voltage on the structure of Ti-doped a-C:H films deposited by FCVA, Appl. Surf. Sci. 253 (2007) 3722–3726, https://doi.org/10.1016/j.apsusc.2006.08.003.

[23] A. Dulmaa, F.G. Cougnon, R. Dedoncker, D. Depla, On the grain size-thickness correlation for thin films, Acta Mater. 212 (2021), https://doi.org/10.1016/j.actamat.2021.116896.

[24] D. Dellasega, F. Mirani, D. Vavassori, C. Conti, M. Passoni, Role of energetic ions in the growth of fcc and ω crystalline phases in Ti films deposited by HiPIMS, Appl. Surf. Sci. 556 (2021), https://doi.org/10.1016/j.apsusc.2021.149678.

[25] P. Panjan, A. Drnovšek, P. Gselman, M. Čekada, M. Panjan, Review of growth defects in thin films prepared by PVD techniques, Coatings 10 (2020), https://doi.org/10.3390/coatings10050447.

[26] T. Mori, S. Fukuda, Y. Takemura, Improvement of mechanical properties of Ti/TiN multilayer film deposited by sputtering, Surf. Coating. Technol. 140 (2001) 122–127, https://doi.org/10.1016/s0257-8972(01)01021-0.

[27] Y. Hoshi, E. Suzuki, H. Shimizu, Control of crystal orientation of Ti thin films by sputtering, Electrochim. Acta 44 (1999) 3945–3952, https://doi.org/10.1016/s0013-4686(99)00103-6.

[28] M.S. Kabir, Z. Zhou, Z. Xie, P. Munroe, Designing multilayer diamond like carbon coatings for improved mechanical properties, J. Mater. Sci. Technol. 65 (2021) 108–117, https://doi.org/10.1016/j.jmst.2020.04.077.

[29] H. Oettel, R. Wiedemann, Residual stresses in PVD hard coatings, Surf. Coating. Technol. 76–77 (1995) 265–273, https://doi.org/10.1016/0257-8972(95)02581-2.

[30] P.R. Guduru, E. Chason, L.B. Freund, Mechanics of compressive stress evolution during thin film growth, J. Mech. Phys. Solid. 51 (2003) 2127–2148, https://doi.org/10.1016/j.jmps.2003.09.013.

[31] J. Wu, Y. Chen, Z. Du, H. Xie, S. Liu, Q. Peng, K. Li, Enhancing the elevated temperature strength of titanium matrix composites through a novel (α + β) TRIPLEX heat treatment, Mater. Sci. Eng., A 890 (2024), https://doi.org/10.1016/j.msea.2023.145884.

[32] D. Wang, S.S. Lin, Q. Shi, Y.N. Xue, H.Z. Yang, D.C. Zhang, Z.Z. Xu, C.Q. Guo, M. J. Dai, B.L. Jiang, K.S. Zhou, Microstructure effects on fracture failure mechanism of CrAl/CrAlN coating, Ceram. Int. 47 (2021) 3657–3664, https://doi.org/10.1016/j.ceramint.2020.09.217.

[33] F. Zhang, C. Li, M. Yan, J. He, Y. Yang, F. Yin, Microstructure and nanomechanical properties of co-deposited Ti-Cr films prepared by magnetron sputtering, Surf. Coating. Technol. 325 (2017) 636–642, https://doi.org/10.1016/j.surfcoat.2017.07.005.

[34] S. Su, W. Chen, M. Zheng, G. Lu, W. Tang, H. Huang, D. Qu, Facile fabrication of 3D-Printed porous Ti6Al4V scaffolds with a Sr-CaP coating for bone regeneration, ACS Omega 7 (2022) 8391–8402, https://doi.org/10.1021/acsomega.1c05908.